

The chosen few: the low mass halos that host faint galaxies

Till Sawala^{1*}, Carlos S. Frenk¹, Azadeh Fattahi², Julio F. Navarro², Tom Theuns^{1,3}, Richard G. Bower¹, Robert A. Crain⁴, Michelle Furlong¹, Adrian Jenkins¹, Matthieu Schaller¹ and Joop Schaye⁴

¹*Institute for Computational Cosmology, Department of Physics, University of Durham, South Road, Durham DH13LE, UK*

²*Department of Physics and Astronomy, University of Victoria, 3800 Finnerty Road, Victoria, British Columbia V8P 5C2, Canada*

³*Department of Physics, University of Antwerp, Campus Groenenborger, Groenenborgerlaan 171, B-2020 Antwerp, Belgium*

⁴*Leiden Observatory, Leiden University, Postbus 9513, 2300 RA Leiden, The Netherlands*

Accepted 2014 ***. Received 2014 ***; in original form 2014

ABSTRACT

Since reionization prevents star formation in most halos less massive than $3 \times 10^9 M_\odot$, dwarf galaxies only populate a fraction of existing dark matter halos. We use hydrodynamic cosmological simulations of the Local Group to study the discriminating factors for galaxy formation in the early Universe and connect them to the present-day properties of galaxies and halos. A combination of selection effects related to reionization, and the subsequent evolution of halos in different environments, introduces strong biases between the population of halos that host dwarf galaxies, and the total halo population. Halos that host galaxies formed earlier and are more concentrated. In addition, halos more affected by tidal stripping are more likely to host a galaxy for a given mass or maximum circular velocity, v_{max} , today. Consequently, satellite halos are populated more frequently than field halos, and satellite halos of $10^8 - 10^9 M_\odot$ or v_{max} of $12 - 20 \text{ km s}^{-1}$, similar to the Local Group dwarf spheroidals, have experienced a greater than average reduction in both mass and v_{max} after infall. They are on closer, more radial orbits with higher infall velocities and earlier infall times. Together, these effects make dwarf galaxies highly biased tracers of the underlying dark matter distribution.

Key words: cosmology: theory – galaxies: formation – galaxies: evolution – galaxies: mass functions – methods: N-body simulations

*“There are some who are in darkness
And the others are in light
And you see the ones in brightness
Those in darkness drop from sight”*

– Bertolt Brecht, *The Threepenny Opera*

surprise that the total number of substructures predicted in a given cosmological model can be far greater than the number of observable galaxies. However, as reionization occurs in the early universe when halos are at a fraction of their final mass, it is also expected that the properties of Local Group halos and galaxies today are only loosely related to the conditions which separated those progenitor halos that were able to form stars from those that have remained dark.

In this paper we examine how the sparse sampling of halos by galaxies in the presence of an ionizing background, and the subsequent evolution of halos and galaxies in a Local Group environment, can lead to a population of halos hosting faint galaxies that is very different from the total halo population.

Previous simulations have studied the impact of reionization both for individual dwarf galaxies and for satellites of Milky Way sized halos. Okamoto et al. (2008) and Okamoto & Frenk (2009) have found that reionization can remove most of the baryons from halos with low maximum circular

1 INTRODUCTION

The Local Group dwarf galaxies and their halos are often described as ideal test cases for the impact of cosmological models on small scale structures. It has, of course, long been recognised that astrophysical processes such as reionization can suppress star formation in low mass halos (e.g. Efstathiou 1992; Bullock et al. 2000; Benson et al. 2002; Somerville 2002). It should therefore perhaps come as no

* E-mail: till.sawala@durham.ac.uk

velocity, v_{\max} (the circular velocity measured at the radius where $v_{\text{circ}} = \sqrt{GM(<r)/r}$ is maximal), and showed that dark satellite halos are expected around the Milky Way with v_{\max} up to 25 km s^{-1} . They concluded that $v_{\max} \sim 12 \text{ km s}^{-1}$ at the time of reionization ($z = 8$ in their model) sharply separates dark and luminous halos. Nickerson et al. (2011) have also performed a simulation of a Milky-Way mass halo and its satellites, but found the peak mass, M_{peak} , which satellites reach during their evolution to be the discriminating factor, with halos of $M_{\text{peak}} < 2 \times 10^9 M_{\odot}$ losing most of their gas to reionization and failing to form stars. Shen et al. (2013) simulated galaxy formation in seven halos of mass between 4.4×10^8 and $3.6 \times 10^{10} M_{\odot}$, and found that the three halos with a peak value of $v_{\max} < 16 \text{ km s}^{-1}$ were devoid of stars, and two halos with peak mass of 1.8 and $3.3 \times 10^9 M_{\odot}$ only started star formation at $z \sim 0.5$, long after reionization.

Recently, we used a set of cosmological hydrodynamic simulations of Local Group like volumes to show that the appearance of “dark” halos that host no galaxy, combined with the reduction in halo mass due to baryonic processes, can significantly change the expected stellar-to-total mass relation of dwarf galaxies, and resolve previously reported discrepancies between observations of individual dwarf galaxies and the predictions of Λ CDM derived from abundance matching (Sawala et al. (2014), see also Sawala et al. (2011)). In this paper we use the same set of simulations to study how reionization selects between halos that host galaxies and those that do not. Following the formation and evolution of dark and luminous halos throughout cosmic time, we can connect their properties in the early universe to the observable galaxies and halos of the present day.

We also link individual halos from the hydrodynamic simulations to their counterparts in dark matter only (DMO) simulations of the same volumes. This allows us to study the intrinsic properties of halos which determine galaxy formation, and distinguish them from the impact that the baryonic processes associated with galaxy formation can have on individual halos. Finally, by comparing the populations of dark and luminous halos in the simulated Local Group volumes, we deduce the biases which can arise when observed galaxies are assumed to be representative of the underlying population of dark matter halos.

This paper is organised as follows. In Section 2, we briefly describe the simulations and the astrophysical assumptions made. By comparing simulations with and without reionization, we discuss the impact of reionization in Section 3. Section 4 describes galaxy formation in the presence of reionization. In Section 4.1, we explain how the assembly histories separate those halos which form stars from those that remain dark. In Section 4.2 we discuss the resulting bias in formation redshifts, and in Section 4.3 we show the difference in concentration between luminous and non-luminous halos. In Section 5, we examine how the subsequent evolution in different environments within the Local Group creates further biases between luminous and non-luminous halos: satellites halos that are luminous have higher infall redshifts and more radial orbits with higher infall velocities (Section 5.1), and the distributions of luminous and non-luminous halos differ within the Local Group (Section 5.2). We discuss some implications of our findings and conclude with a summary in Section 6.

Table 1. Numerical parameters of the simulations

Label	Type	Particle Masses		Max Softening [pc]
		DM [M_{\odot}]	Gas [M_{\odot}]	
L1	hydro	5.0×10^4	1.0×10^4	94
L1	DMO	6.0×10^4	–	94
L2	hydro	5.9×10^5	1.3×10^5	216
L2	DMO	7.2×10^5	–	216
L3	hydro	7.3×10^6	1.5×10^6	500
L3	DMO	8.8×10^6	–	500

2 METHODS

The simulations used in this paper have previously been described in Sawala et al. (2014). We reproduce here the main aspects of their initial conditions and astrophysical model.

We resimulate 12 cosmological volumes as “zoom” simulations extracted from the DOVE simulation, a 100^3 Mpc^3 N-Body simulation based on the WMAP-7 cosmology. We require that each volume should contain two halos of mass in the range $(5 \times 10^{11} - 2.5 \times 10^{12}) M_{\odot}$ separated by $800 \pm 200 \text{ kpc}$, approaching with radial velocity of $(0 - 250) \text{ km s}^{-1}$ and with tangential velocity below 100 km s^{-1} in an environment with an unperturbed Hubble flow out to 4 Mpc. The high resolution initial conditions were created using second-order Lagrangian perturbation theory, as described by Jenkins (2010). The selection of Local Group environments is discussed in more detail in Fattahi et al. (2014, in prep).

The simulations were performed using a pressure-entropy variant (Hopkins 2013) of the Tree-PM SPH code P-GADGET3 (Springel 2005), described in Dalla Vecchia et al. 2014 (in prep.). The subgrid physics model is that of the *Evolution and Assembly of GaLaxies and their Environments* project (EAGLE, Schaye et al. 2014 in prep., Crain et al. 2014 in prep.). It includes metal-dependent radiative cooling (Wiersma et al. 2009) and photo-heating in the presence of UV and X-ray backgrounds, and the cosmic microwave background (CMB).

Prior to reionization, net cooling rates are computed from the CMB and from a UV and X-ray background that follows the $z = 9$ model of Haardt & Madau (2001) with a 1 Ryd high-energy cutoff. To account for the temperature boost due to radiative transfer and non-equilibrium effects over the optically thin limit assumed in our simulations (Abel & Haehnelt 1999), we inject 2 eV per hydrogen and helium atom. We assume that hydrogen reionizes instantaneously at $z = 11.5$ (Planck Collaboration et al. 2013), while the redshift dependence of helium reionization is modelled as a Gaussian centred at $z = 3.5$ (Theuns et al. 2002) with $\sigma(z) = 0.5$. As shown by Wiersma et al. (2009) and Rollinde et al. (2013), the resulting evolution of the temperature-density relation is consistent with measurements of the intergalactic medium (Schaye et al. 2000).

Star formation follows the formulation of Schaye & Dalla Vecchia (2008) with a metallicity-dependent threshold (Schaye 2004). The model includes stellar evolution (Wiersma et al. 2009) and stochastic thermal supernova feedback (Dalla Vecchia & Schaye 2012), as well as black-hole growth and AGN feedback (Rosas-Guevara et al. 2013; Booth & Schaye 2009; Springel et al. 2005).

All simulations were run twice: once with gas and the

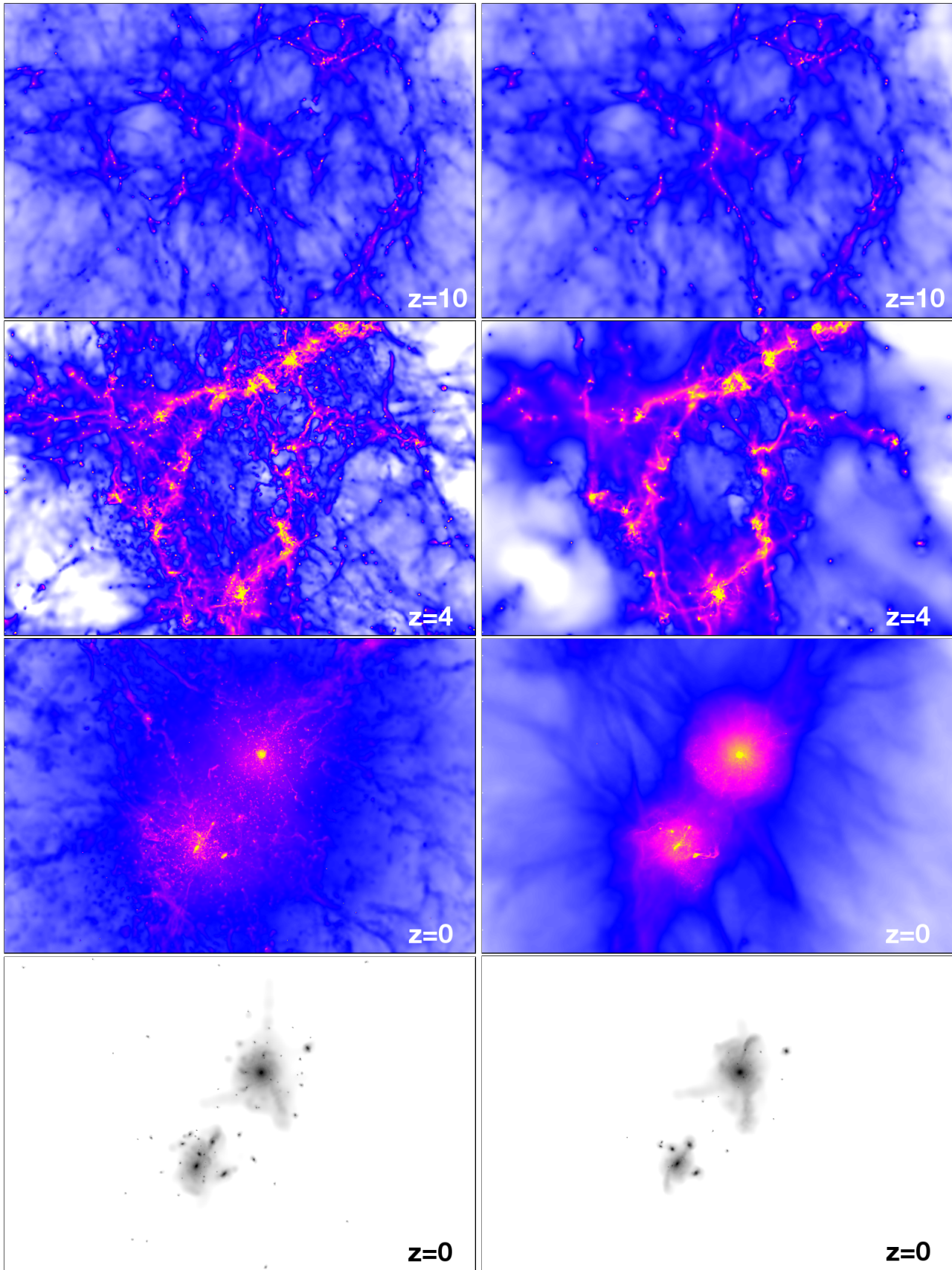


Figure 1. Gas density distribution (top three rows) and stellar density distribution (bottom row, only halos with $m_* > 4 \times 10^6 M_\odot$) in the L2 simulation without reionization (left) and the same volume with reionization (right). The region shown measures $3 \times 2 \text{Mpc}^2$ at $z = 0$ and is magnified proportional to $a(z)$ at higher redshifts. Following reionization at $z = 11.5$, gas is removed from low mass halos, and reduced cooling results in a less fragmented IGM. The impact of reionization is first noticeable in the low-density regions, which are already less structured at $z = 10$, just after reionization. At later times, the differences increase, and the number of collapsed and eventually star-forming halos is much lower in the simulation that includes reionization.

baryon physics described above, and once as dark matter only (DMO). In addition, one volume was also run with the complete hydrodynamic model, but without reionization. In the DMO simulations the dark matter particle masses are larger by a factor of $(\Omega_b + \Omega_{DM})/\Omega_{DM}$ relative to the corresponding hydrodynamic simulations. To investigate the regime of Local Group dwarf galaxies, we use three different resolution levels labelled L1, L2 and L3, whose parameters are given in Table 1. In this work, L3 is only used to test convergence. The main results for the model that includes reionization are obtained from five pairs of hydrodynamic and DMO simulations at resolution L2 and one pair at L1. The simulations without reionization presented in Section 3 were only run up to L2.

We use a Friends-of-Friends algorithm (FoF; Davis et al. 1985) to identify overdense structures (FoF-groups), and the SUBFIND algorithm (Springel et al. 2001; Dolag et al. 2009) to identify self-bound substructures within them. As they represent the objects most directly associated with individual galaxies, we always refer to the self-bound substructures as “halos”. The principal substructure within an FoF-group contains most of its mass, but satellites may share the same FoF-group while still residing in separate self-bound halos. Throughout this paper, we use the term “satellite” when we refer to the satellite halos or galaxies associated with the M31 and Milky-Way analogues, and “field” when we refer to isolated halos.

We analyse our simulations at 128 snapshots, and trace the evolution of individual halos in both the hydrodynamic and DMO simulations using merger trees, as described in Helly et al. (2003) and Qu et al. (2014, in prep.). The unique IDs of dark matter particles which encode their positions in the initial conditions allow us to match and compare individual halos from different simulations of the same volume at the same resolution.

3 THE IMPACT OF REIONIZATION

From $z = 11.5$, the UV background heats the intergalactic medium and lowers its cooling rate. It can also remove gas from low-mass halos by photo-evaporation. In Fig. 1 we compare the evolution of the gas density distributions in two simulations of the same volume and resolution (L2) with and without reionization, as well as the final stellar density distribution. At $z = 10$, shortly after hydrogen reionization, the main difference is apparent in the low-density regions. Here, the thermal energy provided by reionization slows the collapse of small structures which results in a smoother IGM than in the absence of reionization. By comparison, regions of higher density which correspond to halos that have already formed before reionization, are not significantly affected. By $z = 4$, the intergalactic medium has become significantly more fragmented in the simulation without reionization, with many more low-mass halos now containing dense gas and forming stars compared to the simulation with reionization. At $z = 0$ it can be seen that while the large-scale features in both the gas- and stellar density distributions are similar, in the absence of reionization, the IGM is strongly fragmented and has collapsed into many small clumps. By contrast, the IGM in the simulation with reionization has remained much smoother. Without reion-

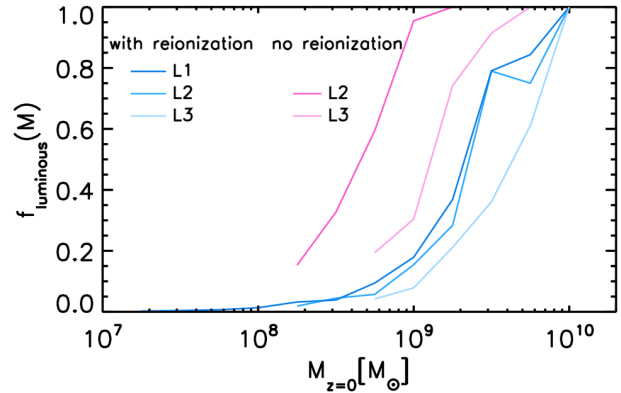


Figure 2. Fraction of halos which are luminous at $z = 0$ as a function of halo mass in simulations with and without reionization for different resolutions. When reionization is included, the fraction of luminous halos as a function of mass is much reduced. In the simulation with reionization, the luminous fraction is converged at L2. By contrast, without reionization, the luminous fraction is not numerically converged, and would increase further with higher resolution.

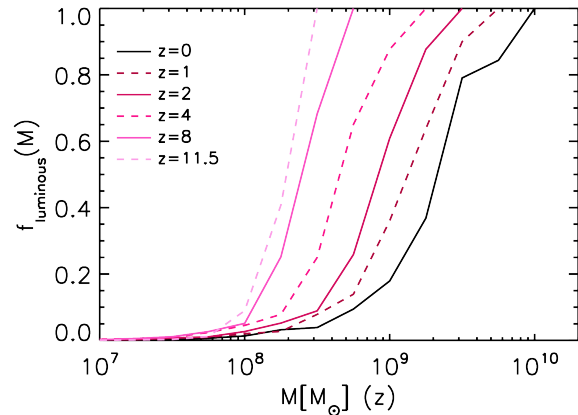


Figure 3. Fraction of halos which are luminous as a function of halo mass at different redshifts from $z = 11.5$ to $z = 0$ in the simulation with reionization at resolution L1. At any redshift, the fraction of luminous halos of mass below $10^8 M_\odot$ is less than 10%, and almost no halos below $10^{7.5} M_\odot$ contain stars. The mass scale that separates luminous from dark halos evolves from $\sim 3 \times 10^8 M_\odot$ at $z = 11.5$ to $\sim 3 \times 10^9 M_\odot$ at $z = 0$.

ization, the number of halos within 2.5 Mpc from the LG centre that contain stars is ~ 700 , compared to only ~ 180 in the same volume with reionization.

In Fig. 2 we compare the fraction of halos containing stars at $z = 0$, for simulations of the same volume with and without reionization and at different resolutions, as defined in Table 1. It can be seen that significantly more halos are luminous in the simulations without reionization. It should be noted that our simulations are not sufficient to simulate a Universe without reionization faithfully: the level of fragmentation of the IGM is limited by resolution, and the total number of galaxies formed in this (unphysical) scenario is not converged and increases with increasing resolution. By contrast, the results with reionization are well converged at L2, suggesting that in our simulations, reionization sets a

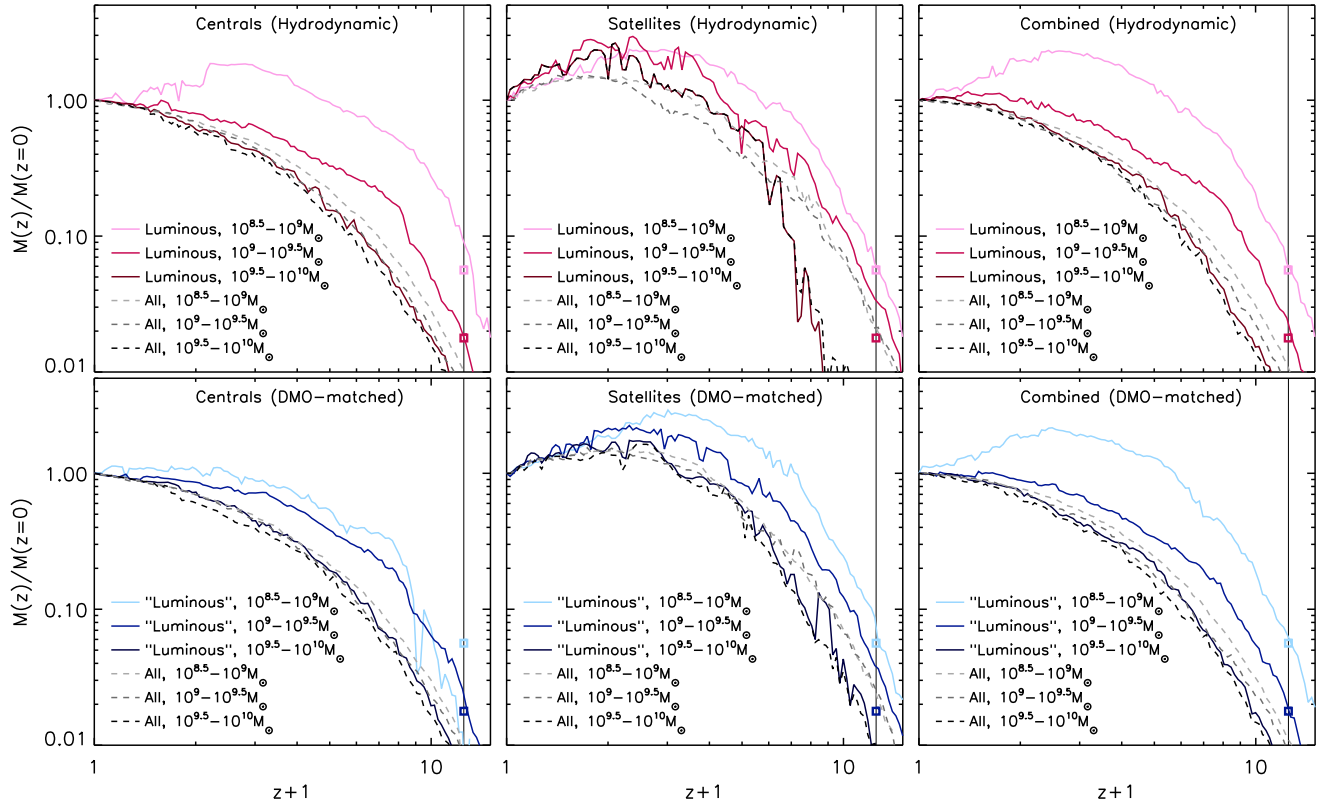


Figure 4. Mass assembly history for present-day field halos (left), present-day satellites (centre), and the combination of both (right). Halos are grouped according to mass at $z = 0$, as measured in the hydrodynamic simulation (top row), and as measured in the DMO simulation (bottom row). The vertical lines indicate $z = 11.5$, the time of hydrogen reionization, and the squares indicate mass ratios that corresponds to the same halo mass ($10^{7.5}M_{\odot}$) at this time for each final mass bin. As indicated by the dashed lines, halos of lower final mass generally formed earlier, but this trend is greatly amplified for luminous halos. With decreasing final mass, luminous halos become increasingly biased towards earlier formation times. Tidal stripping typically results in mass loss for satellites, whereas field halos tend to reach their peak mass at $z = 0$. However, note that luminous field halos with masses below 10^9M_{\odot} today are also likely to have been tidally stripped in the past, leading to an evolution more similar to that of satellites.

limit for star formation in low mass halos that is above the resolution limit of our simulations.

Fig. 3 shows the evolution of the luminous fraction of halos as a function of mass in a simulation that includes reionization, from $z = 11.5$ to $z = 0$. At all redshifts, the fraction of luminous halos at 10^8M_{\odot} is less than 10%, and almost no halos are luminous below $10^{7.5}M_{\odot}$. The mass-dependence of the luminous fraction is strongest at $z = 11.5$, where all halos more massive than $3 \times 10^8M_{\odot}$ contain stars. As halos typically grow in mass over time, the mass-dependence of the luminous fraction becomes more gradual towards lower redshifts. While the minimum halo mass of luminous halos remains almost unchanged, the mass at which most halos are luminous increases continuously.

Of course, supernovae and AGN feedback can also heat up the gas and regulate star formation in larger halos. However, reionization is clearly a key factor for determining the total number of galaxies that form and can also strengthen the impact of supernovae on the star formation rate (Pawlik & Schaye 2009). In terms of the halo properties required for star formation in the presence of reionization, our results are consistent with those obtained by the previous studies reviewed in Section 1. At a mass of $\sim 3 \times 10^9M_{\odot}$, or $v_{\text{max}} \sim 25 \text{ km s}^{-1}$, half of all halos contain galaxies at $z = 0$.

4 THE TIMING OF GALAXY FORMATION

Since reionization takes place at a time when halos have only a small fraction of their present mass, the probability for star formation within a halo is expected to depend strongly on its individual assembly history. Consequently, the properties that separate the halos that host galaxies from those that remain dark should be more closely related to their progenitors at high redshifts.

Halos that have assembled more mass at the time of reionization will be more resilient to photo-evaporation, and will subsequently be able to cool gas more efficiently, resulting in a greater chance for star formation. As a result, for a fixed mass today, halos that formed earlier are more likely to contain galaxies, so that halos that host galaxies are biased towards earlier formation times.

4.1 Assembly Histories

In Fig. 4 we compare the average mass assembly histories of luminous and dark halos in three different final halo mass ranges. We distinguish between presently isolated halos and satellites, and compare the results measured directly in the hydrodynamic simulation to those measured by comparing the matched counterparts to the luminous and non-luminous halos from the dark matter only (DMO) simulation.

As expected, we find that halos which form stars assemble their mass significantly earlier compared to non-luminous halos of the same mass today.

We reproduce the well-known result of hierarchical structure formation that halos of lower mass typically form earlier than halos of larger mass, independently of whether or not they contain stars. Since most halos above $10^{9.5}M_{\odot}$ are luminous, we find only a slight difference between the assembly histories of dark and luminous halos above this mass. However, as the fraction of luminous halos decreases in the mass ranges $10^9 - 10^{9.5}M_{\odot}$ and $10^{8.5} - 10^9M_{\odot}$, the remaining luminous halos are increasingly biased towards earlier mass assembly. This result can be readily understood from the fact that for gas cooling and star formation to take place in the presence of reionization, a sufficiently high mass needs to have been assembled at an early time.

It is worth pointing out that while low mass halos have to assemble their mass early in order to survive reionization, star formation itself begins later for most halos. Of all halos that contain galaxies at $z = 0$, only $\sim 8\%$ have started forming stars before $z = 11.5$, with a median redshift of $z = 6$ for the first stars to form in each galaxy.

As shown in the middle column of Fig. 4, luminous as well as dark satellites of all masses have typically experienced some degree of tidal stripping and mass loss, leading to a decrease in average mass towards $z = 0$. By comparison, the mass of present-day field halos is typically maximal at $z = 0$. However, the least massive luminous field halos in the hydrodynamic simulation achieved their peak mass at $z > 0$, and have since lost mass as a result of tidal interactions. Note that the combination of strong stripping and ejection means that a pair of matched halos is unlikely to evolve in the same way across in the hydrodynamic and DMO simulations, and that low mass centrals in the DMO simulation are more likely to be matched to slightly more massive centrals in the hydrodynamic simulation than to be on such a rare orbit. However, while such objects are rare amongst all halos, star formation in halos with peak mass of less than 10^9M_{\odot} is also rare, so the probability of an isolated galaxy in such a low mass halo having had such an exceptional history is strongly increased.

In this context, it is also worth noting that Teyssier et al. (2012) have computed the probability that halos of isolated dwarf galaxies within the Local Group are “escaped” satellites, based on orbits of halos measured in the Via Lactea II dark matter only simulation. They found that $\sim 13\%$ of halos within 1.5 Mpc have passed through the Milky Way’s virial radius. Our results suggest that for actual field dwarf galaxies in very low mass halos, the probability of past tidal interactions is significantly higher.

4.2 Formation Redshifts

The difference in assembly history between luminous and non-luminous halos can also be expressed as a bias in formation redshift, $z_{1/2}$, defined as the redshift at which a halo’s most massive progenitor first reaches 1/2 of its peak mass. In Fig. 5, we plot the formation redshifts of luminous and non-luminous halos as a function of their peak mass.

While the total population of halos shows only a weak dependence of formation redshift on mass (in agreement with Fakhouri et al. 2010), the sub-populations of lumi-

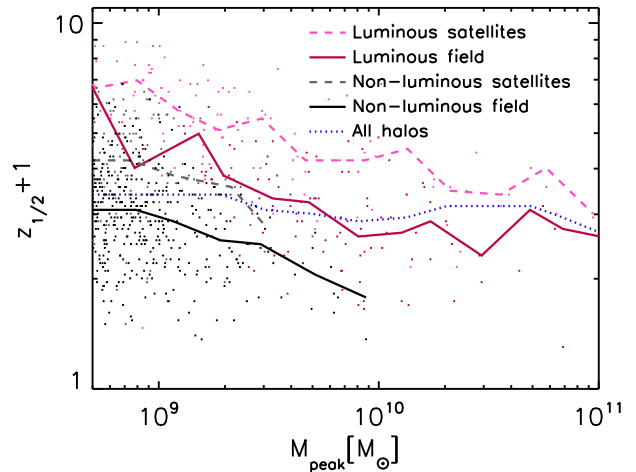


Figure 5. Redshift when a halo reached half of its peak mass as a function of peak mass. Luminous halos which were able to cool stars in the presence of reionization formed significantly earlier than non-luminous ones of the same peak mass. As the required evolution bias increases for lower mass halos, both luminous and dark halos show a strong mass evolution of the formation redshift, whereas the total halo population does not.

nous and non-luminous halos *both* show a strong mass-dependence, with lower mass halos forming earlier. This result can be understood because at any mass, luminous halos form earlier than dark halos: halos of low mass have to form earlier to be luminous, and halos of high mass have to form later to be dark. The increase in the fraction of luminous halos with mass then offsets the negative correlation of mass with formation redshift in each subset to give a total population in which mass and formation time are largely uncorrelated.

The average formation redshift of present-day satellites is higher than that of present-day field halos. Satellite halos typically reach their peak mass at z_{infall} before $z = 0$, while the masses of field halos typically continue to increase to $z = 0$. The exception are present-day field halos that experienced past tidal interactions, which, like satellites, are below their peak mass today. As noted in Section 4.1, among field halos with peak masses below 10^9M_{\odot} that are luminous the probability of such a history is increased significantly.

In summary, we find that the progenitors of present-day dwarf galaxies do not have the assembly histories typical of dark matter halos of their mass or v_{max} . While dark halos of peak mass 10^9M_{\odot} form at $z_{1/2} \sim 2$, halos of the same mass that host galaxies have a formation redshift of $z_{1/2} \sim 3 - 4$.

4.3 Velocity – mass relation

Halos that formed earlier have higher concentration, and therefore higher maximum circular velocity, v_{max} , for a given mass. In addition, more concentrated halos can cool gas more efficiently, limiting the photo-evaporating effect of reionization. Since both early mass growth and the resistance to photo-evaporation enhance the probability for star formation, we expect low-mass galaxies to be hosted preferentially by halos of higher v_{max} – mass ratios.

In Fig. 6 we show the relation between v_{max} and halo mass, either evaluated at $z = 0$ or at z_{peak} , the time of peak

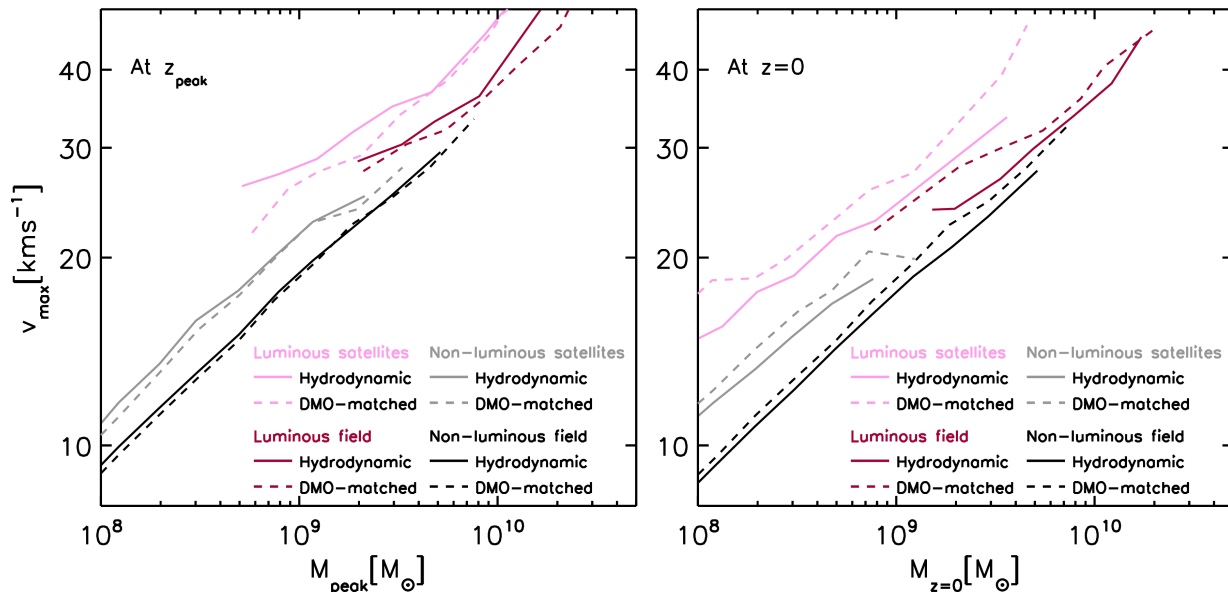


Figure 6. The relation between halo mass and v_{\max} at the time of peak mass (left panel) and at $z = 0$ (right panel) from the simulation at resolution L1 including reionization. Since stars form preferentially in halos of high concentration, luminous halos are on average more concentrated than dark halos. The effect of galaxy formation itself on the halo is manifest in the difference between the relations measured in the hydrodynamic simulation and those measured from the matched DMO simulation. At peak mass, luminous halos in the hydrodynamic simulation have higher v_{\max}/mass ratios than their DMO counterparts, indicating that gas cooling leads to an increase in concentration. At $z = 0$ halos of all type are typically less concentrated in the hydrodynamic simulation than in the DMO simulation.

mass. While the total population follows the $v_{\max} - \text{mass}$ relations expected for ΛCDM (e.g. Klypin et al. 2011, not shown), we find that below $10^{9.5}M_{\odot}$, luminous halos have significantly higher $v_{\max} - \text{mass}$ ratios than non-luminous ones. As the fraction of luminous halos in our hydrodynamic simulation decreases with decreasing halo mass, the bias of the remaining luminous halos increases. Similarly, at high masses where most halos are luminous, the remaining dark halos are increasingly biased towards lower $v_{\max} - \text{mass}$ ratios.

We find similar trends when we consider the halos of the DMO simulation that are matched to luminous and non-luminous halos. Like the luminous halos themselves, their counterparts in the DMO simulation have much higher $v_{\max} - \text{mass}$ ratios than the DMO counterparts of the non-luminous halos. This confirms that the increased v_{\max} of luminous halos in the hydrodynamic simulation is largely explained by the fact that more concentrated halos are intrinsically more likely to form stars.

We can examine the additional effect of baryons by directly comparing the $v_{\max} - \text{mass}$ relation between halos in the hydrodynamic simulation and their respective DMO counterparts. From the left panel of Fig. 6, it can be seen that at peak mass, the non-luminous halos and their DMO counterparts follow very similar relations, while the luminous halos in the hydrodynamic simulation are more concentrated than their DMO counterparts. This indicates that processes like gas cooling, which are stronger in the luminous than in the non-luminous halos, can also lead to an increase in the $v_{\max} - \text{mass}$ ratios, an effect obviously not present in the DMO simulation.

When the two simulations are compared at $z = 0$, as is the case in the right panel of Fig. 6, luminous and non-luminous halos alike have lower average $v_{\max} - \text{mass}$ ratios than their respective counterparts in the DMO simula-

tion. However, this difference is small compared to the offset between luminous and dark halos or the corresponding matched objects.

It can also be seen that satellites follow a different $v_{\max} - \text{mass}$ relation compared to field halos, with a lower mass for a given v_{\max} . This well-known result can be attributed to the fact that tidal stripping first removes material from the outside of an infalling halo, beyond r_{\max} , with a greater impact on halo mass than on v_{\max} . However, we also find that the difference between satellite and field halos is strongly amplified among luminous halos because, as we will discuss in Section 5.1, luminous and dark satellites follow significantly different orbits.

In summary, we find that luminous low-mass halos have much higher $v_{\max} - \text{mass}$ ratios than average halos. This difference increases as the fraction of luminous halos decreases towards lower masses, and is higher for satellites than for field halos. Since we find similar trends between the respective matched halos in DMO simulation, we attribute them mostly to the increased likelihood for star formation in more concentrated halos, rather than to an increase of concentration due to cooling and star formation.

5 LATE TIME EVOLUTION

In addition to the effects of assembly history and the properties of halos directly related to reionization, the late-time evolution also influences the probability for halos to host galaxies, and the expected distribution of luminous and dark halos within the Local Group.

In the previous section, we showed that the progenitors of luminous halos formed significantly earlier than those of dark halos. We also noted clear differences between the evolution of satellites and centrals. These are not a direct

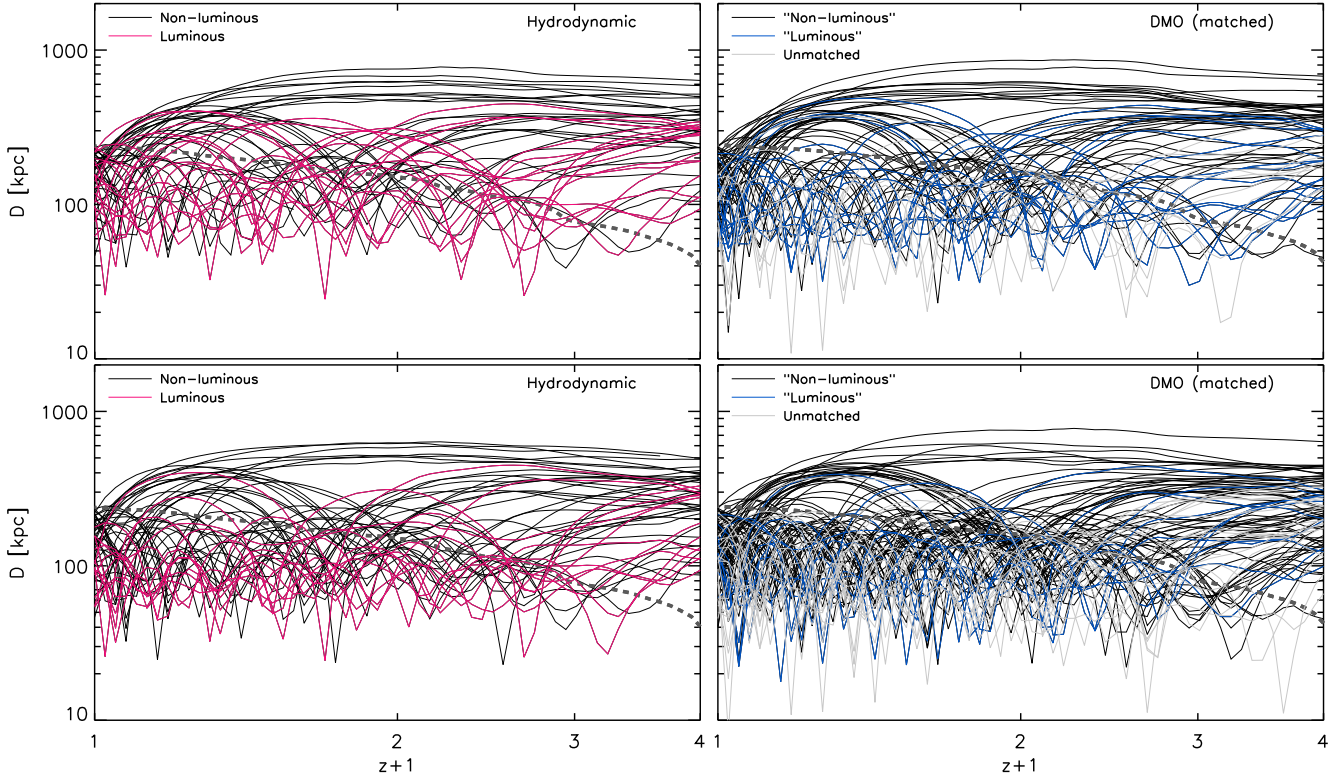


Figure 7. Evolution of galactocentric distance for dark and luminous satellites of the simulated “Milky Way”, as identified directly in the hydrodynamic simulation (left column), or as matched from the DMO simulation (right column) at resolution L1. Satellite halos are selected by present mass in the range $10^8 - 10^9 M_{\odot}$ (top row) or present v_{\max} in the range $12 - 20 \text{ km s}^{-1}$ (bottom row). In each panel, the grey dashed line shows the evolution of the host halo’s virial radius, r_{200} , in both simulations. Within this range of mass or v_{\max} , the orbits of luminous and dark halos differ significantly. Also note the lower number of objects in the hydrodynamic simulation compared to the DMO simulation, due to the reduction of v_{\max} and mass of individual halos by baryonic effects.

consequence of reionization, but indicate that differences in the late-time evolution can change the correspondence between the properties of present-day halos and those of their progenitors in the early universe.

In this section, we examine the late-time effects in more detail, and show in particular how tidal stripping and the fact that satellites stop growing after infall, can introduce a strong environmental dependence on the relation between observable galaxies and the underlying halo population.

5.1 Satellite Evolution

The evolution of satellite halos is driven by tidal effects, which further separate their present-day properties from those of their progenitors. Among satellite halos of the same mass or v_{\max} today, those that experienced greater mass loss had more massive progenitors prior to infall, and therefore a higher probability for star formation. This introduces additional biases between dark and luminous satellites that depend on their infall times and orbital parameters.

In Fig. 7 we compare the orbits of luminous and dark low-mass satellites of one of our simulated Milky-Way like halos. We identify satellites as self-bound halos within the virial radius of the host at $z = 0$, r_{200} , defined as the radius within which the mean density is $200 \times$ the *critical* density, and define the infall redshift, z_{infall} , as the redshift when a satellite first crosses r_{200} . Selecting satellites either by their present mass or present v_{\max} , it can be seen that the orbits

of luminous halos in the mass range of $10^8 - 10^9 M_{\odot}$ or the v_{\max} range of $12 - 20 \text{ km s}^{-1}$ differ significantly from those of dark halos of the same present mass: they fall in earlier and come closer to the centre of the host.

We note that the same effect can be seen between the halos of the DMO simulation which are matched to luminous and dark halos in the hydrodynamic simulation and shown in the right column of Fig. 7. The matching of low mass satellites is imperfect because satellites can evolve differently in the two simulations. Nevertheless, it underlines the fact that the different orbits of luminous and non-luminous satellites are primarily caused by a selection effect of the progenitors imposed by reionization, and not by differences in the baryonic components between the luminous and dark satellites. However, the overall number of satellites is reduced in the hydrodynamic simulation due to the loss of baryons, consistent with the results of Sawala et al. (2013).

Fig. 8 shows the distribution of infall redshifts of luminous and non-luminous satellites in the v_{\max} range of $12 - 20 \text{ km s}^{-1}$, comparable to the values inferred for the halos that host the Milky Way dwarf spheroidal galaxies. These results include satellites of all 10 M31 and Milky Way like halos in our five Local Group simulations at resolution L2. The median infall redshift of non-luminous satellites in this v_{\max} range is 1.0, while luminous satellites fell in significantly earlier, with a median infall redshift of 1.5.

It is worth noting that in addition to *mass loss* through tidal stripping, the infall of a satellite also marks the end

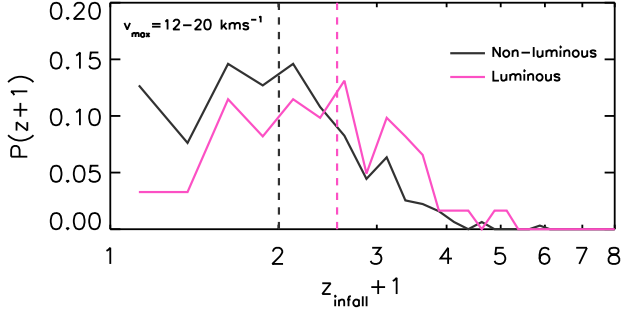


Figure 8. Distributions of infall redshifts of luminous and non-luminous satellites in the present-day v_{\max} range of $12\text{--}20\text{ km s}^{-1}$. The dashed lines indicate the median values. Luminous halos of these v_{\max} values fell in significantly earlier than non-luminous halos.

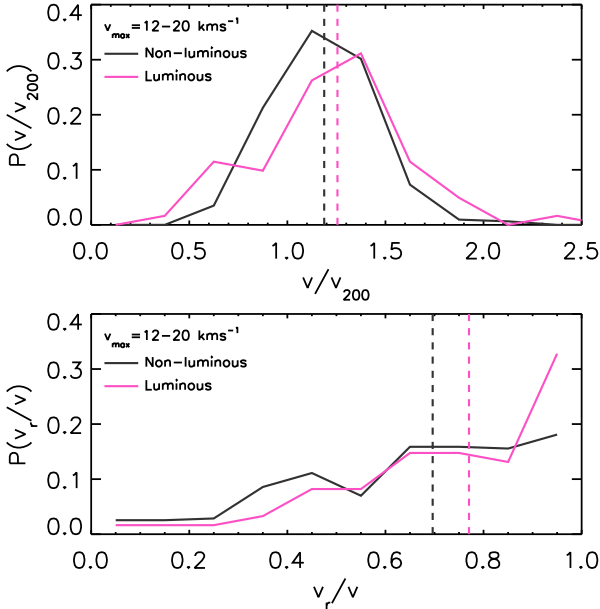


Figure 9. Top panel: distributions of infall velocities of satellites in the present-day v_{\max} range of $12\text{--}20\text{ km s}^{-1}$ divided by v_{200} of the host halo at the time of infall. Bottom panel: distributions of the ratio between the radial component and the total infall velocity. On both panels, the dashed lines indicate the median values. Luminous halos in this v_{\max} range fell in with slightly higher velocities and on more radial orbits compared to non-luminous halos.

of *mass growth* that a field halo would typically experience. For the same infall mass, an earlier infall time corresponds to a higher mass in the early universe, further enhancing the probability of star formation.

In Fig. 9 we compare the same population of satellites described above in terms of the ratio between the infall velocity of the satellite and the virial velocity of the host halo, v/v_{200} , at the time of infall, and in terms of the ratio between the radial component and the total infall velocity, v_r/v . Again, we find that luminous satellites in this v_{\max} -range fell in with slightly higher infall velocities and on more radial orbits, both of which made them more susceptible to tidal stripping.

The post-infall changes in mass and v_{\max} among luminous and dark satellites as functions of present mass and

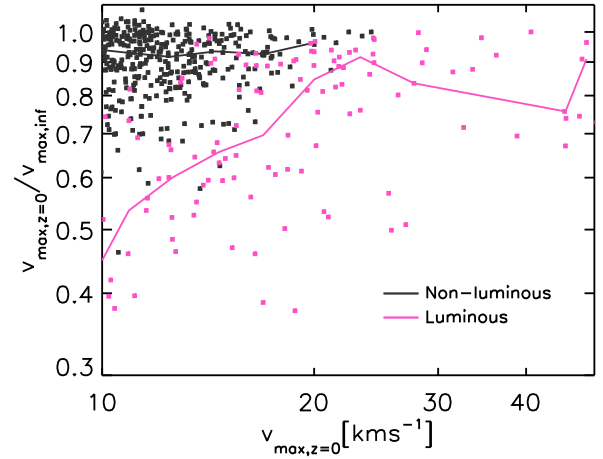
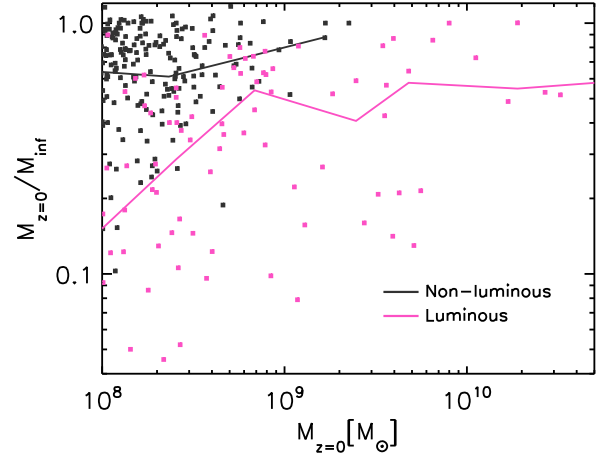


Figure 10. Change in mass relative to mass at z_{infall} as a function of present mass (top panel), and change in v_{\max} relative to v_{\max} at z_{infall} as a function of present v_{\max} (bottom panel), for luminous and non-luminous satellite halos of the parent halo shown in Fig. 7. Lines indicate the median values. As halos with infall masses $< 10^{9.5} M_{\odot}$ or $v_{\max} < 25\text{ km s}^{-1}$ are unlikely to host galaxies, luminous halos with such lower present values are likely to have experienced a much more significant decrease in mass and v_{\max} from their peak values compared to non-luminous halos.

v_{\max} are compared in Fig. 10. As expected, luminous satellites of low present mass are increasingly more likely to have lost mass due to stripping. Whereas dark satellites have typically lost only 1/3 of their mass after infall, independent of present mass, luminous satellites of $10^9 M_{\odot}$ have lost of 1/2 of their mass in the median, a fraction that increases further for lower mass halos. While dark satellites have typically reduced their v_{\max} by less than 10%, luminous satellites of 20 km s^{-1} today have typically experienced a reduction in v_{\max} by 25%.

The bias seen in the infall times, orbits, and reduction in mass and v_{\max} of satellites similar to those that host the observed dwarf spheroidal galaxies may change previous assumptions about their evolution: whereas Peñarrubia et al. (2008) have shown using DMO simulations that the v_{\max} of most dwarf-sized *halos* should not be affected by tidal effects, our simulations show that the opposite is true for the subset of halos that actually host the dwarf spheroidal *galaxies*. Those satellite galaxies that today inhabit halos of $v_{\max} \sim 20\text{ km s}^{-1}$ typically formed in halos of $\sim 30\text{ km s}^{-1}$.

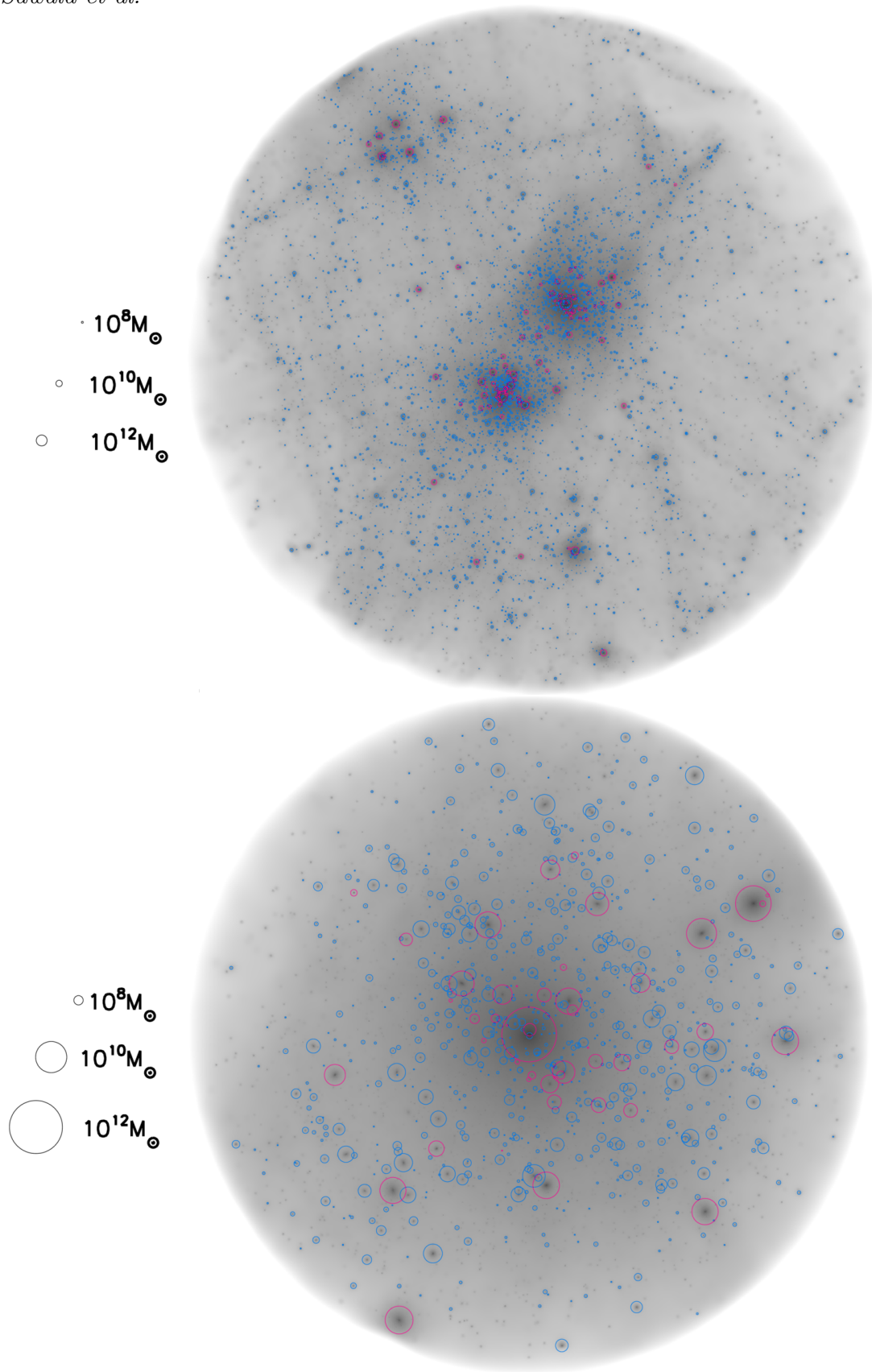


Figure 11. Projected density distribution of dark matter and positions of halos at $z = 0$ in the same simulated Local Group volume as Fig. 1, in a sphere of radius 2 Mpc centred on the LG barycentre (top panel), and a sphere of 400 kpc radius centred on the simulated Milky-Way (bottom panel). Blue and red circles indicate the positions of dark and luminous halos above $10^7 M_{\odot}$, respectively, with diameter proportional to the logarithm of the mass. It can be seen that luminous halos of low mass cluster near the two main halos. Also, while more massive halos are more likely to be luminous, there is no sharp mass threshold separating luminous and dark halos at $z = 0$, since the probability of hosting a galaxy is a function of mass, assembly history, and environment.

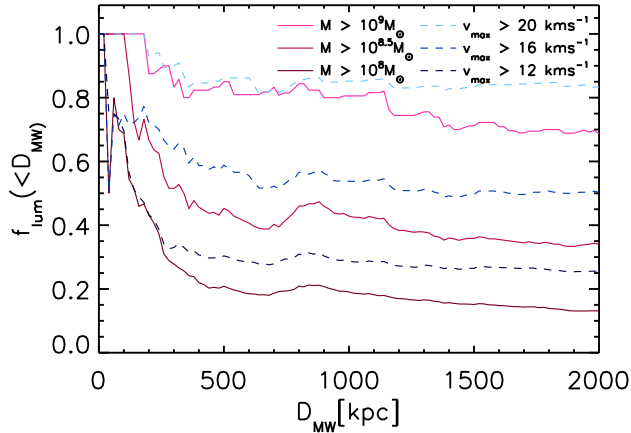


Figure 12. Fraction of halos above a given mass (solid lines) or v_{\max} (dashed lines), within a given distance from the centre of the simulated “Milky Way”. At fixed mass, halos within ~ 300 kpc of the Milky Way are much more likely to contain galaxies than more isolated halos, and the environmental dependence is stronger among halos of lower present mass or v_{\max} .

5.2 Dwarf Galaxies and Halos in the Local Group

The effect of stripping that separates the luminous and non-luminous satellites also extends to a marked difference between satellite and field halos within the Local Group, and differences in the distribution of luminous and dark halos beyond the virial radius of its two main galaxies.

In Fig. 11 we show the $z = 0$ distributions of halos above $10^7 M_{\odot}$ within 2 Mpc to the centre of one of our Local Group volumes, and within 400 kpc of one of the Milky-Way like halos. It can be seen that low-mass luminous halos are predominantly found close to the larger galaxies, where stripping has led to a significant reduction in mass.

While ram pressure stripping can quench star formation and introduce environmental dependencies on the properties of low mass galaxies, gas is not responsible for the environmental dependence of the luminous fraction. It is primarily driven by the fact that, as a result of tidal stripping, halos of a given mass or v_{\max} today that are closer to the central galaxies typically had higher masses or v_{\max} in the early universe, and therefore a higher probability for star formation.

In Fig. 12 we show the fraction of halos of a given mass or v_{\max} today that are populated by galaxies, as a function of distance to the Milky-Way-like galaxy. It can be seen that while all satellites with $M > 10^9 M_{\odot}$ or $v_{\max} > 20 \text{ km s}^{-1}$, as well as a large fraction of lower mass halos, are populated inside 200 kpc, the fraction decreases with increasing distance (an increase at ~ 800 kpc can be attributed to the satellites of the second massive halo in the simulated Local Group, i.e. the halo of “M31”).

This result implies that there are fewer isolated dwarf galaxies in the Local Group than a simple extrapolation based on v_{\max} or mass from the Milky Way and M31 satellites would suggest.

6 DISCUSSION AND SUMMARY

We have analysed a set of hydrodynamic and dark matter only (DMO) simulations of the Local Group in order to study how galaxies populate low mass halos in the presence of reionization. We have shown that reionization greatly reduces the number of dwarf galaxies that form, and that even at fixed mass or v_{\max} today, the subset of halos that host the Local Group’s dwarf galaxies differ significantly from the total halo population.

The differences between the luminous and non-luminous halos result from a combination of early-time and late-time effects. Halos of mass below $\sim 3 \times 10^9 M_{\odot}$ or v_{\max} below $\sim 25 \text{ km s}^{-1}$, that host the majority of the Local Group dwarf galaxies, assembled their mass significantly earlier than typical dark matter halos of the same present-day mass or v_{\max} . Since halos that form earlier are more concentrated, and also because more concentrated halos are more resistant to photo-evaporation, those halos that contain stars have significantly higher v_{\max} – mass ratios.

The late-time evolution of halos, and in particular tidal stripping, introduces further biases between the luminous and non-luminous halos. The halos of satellite galaxies with mass and v_{\max} values similar to those of the observed dwarf spheroidals experienced much stronger tidal stripping than comparable non-luminous satellites. The Milky Way or M31 satellite galaxies typically formed in halos that were more than twice as massive and had significantly higher v_{\max} values prior to infall. They also had earlier infall redshifts, higher infall velocities, and followed more radial orbits than typical dark matter halos.

Within the Local Group, isolated halos are much less likely to host galaxies than satellites of comparable mass or v_{\max} today. In particular, present-day field dwarf galaxies that share the characteristics of dwarf spheroidals are more likely to be “escaped” satellites than was assumed from earlier DMO studies.

The biases between the luminous and non-luminous halos described here have to be taken into account whenever the properties of halos or of the underlying cosmology are to be measured, but only those halos that contain galaxies can be observed.

It is worth noting that our simulations still have several limitations. They assume that reionization is uniform and do not account for local sources of ionization. Radiative transfer is not included, cooling rates are computed in the optically thin limit, star formation is modelled in a stochastic way, and we did not include star formation in mini halos powered by H_2 cooling. While we have shown that the fraction of halos populated by galaxies is numerically converged, it may still depend on model parameters.

With these limitations in mind, we would like to emphasise the importance of the connection between the observable dwarf galaxies and the underlying population of dark matter halos. As noted in the beginning, the Local Group dwarf galaxies provide the best window for studying the nature of dark matter on small scales. However, our results suggest that because reionization leaves most halos empty, Local Group dwarf galaxies today *typically* live in halos that are highly *atypical*.

ACKNOWLEDGEMENTS

We are indebted to Dr. Lydia Heck who ensures that the computers run smoothly at the ICC. This work was supported by the Science and Technology Facilities Council [grant number ST/F001166/1 and RF040218], the European Research Council under the European Union's Seventh Framework Programme (FP7/2007-2013) / ERC Grant agreement 278594-GasAroundGalaxies, the National Science Foundation under Grant No. PHYS-1066293, the Interuniversity Attraction Poles Programme of the Belgian Science Policy Office [AP P7/08 CHARM] and the hospitality of the Aspen Center for Physics. T. S. acknowledges the Marie-Curie ITN CosmoComp. C. S. F. acknowledges an ERC Advanced Investigator Grant COSMIWAY. This work used the DiRAC Data Centric system at Durham University, operated by the Institute for Computational Cosmology on behalf of the STFC DiRAC HPC Facility (www.dirac.ac.uk), and resources provided by WestGrid (www.westgrid.ca) and Compute Canada / Calcul Canada (www.computecanada.ca). The DiRAC system is funded by BIS National E-infrastructure capital grant ST/K00042X/1, STFC capital grant ST/H008519/1, STFC DiRAC Operations grant ST/K003267/1, and Durham University. DiRAC is part of the National E-Infrastructure.

REFERENCES

- Abel T., Haehnelt M. G., 1999, *ApJ*, 520, L13
- Benson A. J., Frenk C. S., Lacey C. G., Baugh C. M., Cole S., 2002, *MNRAS*, 333, 177
- Booth C. M., Schaye J., 2009, *MNRAS*, 398, 53
- Bullock J. S., Kravtsov A. V., Weinberg D. H., 2000, *ApJ*, 539, 517
- Dalla Vecchia C., Schaye J., 2012, *MNRAS*, 426, 140
- Davis M., Efstathiou G., Frenk C. S., White S. D. M., 1985, *ApJ*, 292, 371
- Dolag K., Borgani S., Murante G., Springel V., 2009, *MNRAS*, 399, 497
- Efstathiou G., 1992, *MNRAS*, 256, 43P
- Fakhouri O., Ma C.-P., Boylan-Kolchin M., 2010, *MNRAS*, 406, 2267
- Haardt F., Madau P., 2001, in D. M. Neumann & J. T. V. Tran ed., *Clusters of Galaxies and the High Redshift Universe Observed in X-rays Modelling the UV/X-ray cosmic background with CUBA*
- Helly J. C., Cole S., Frenk C. S., Baugh C. M., Benson A., Lacey C., 2003, *MNRAS*, 338, 903
- Hopkins P. F., 2013, *MNRAS*, 428, 2840
- Jenkins A., 2010, *MNRAS*, 403, 1859
- Klypin A. A., Trujillo-Gomez S., Primack J., 2011, *ApJ*, 740, 102
- Nickerson S., Stinson G., Couchman H. M. P., Bailin J., Wadsley J., 2011, *MNRAS*, 415, 257
- Okamoto T., Frenk C. S., 2009, *MNRAS*, 399, L174
- Okamoto T., Gao L., Theuns T., 2008, *MNRAS*, 390, 920
- Pawlik A. H., Schaye J., 2009, *MNRAS*, 396, L46
- Peñarrubia J., McConnachie A. W., Navarro J. F., 2008, *ApJ*, 672, 904
- Planck Collaboration Ade P. A. R., Aghanim N., Armitage-Caplan C., Arnaud M., Ashdown M., Atrio-Barandela F., Aumont J., Baccigalupi C., Banday A. J., et al. 2013, *ArXiv* 1303.5076
- Rollinde E., Theuns T., Schaye J., Pâris I., Petitjean P., 2013, *MNRAS*, 428, 540
- Rosas-Guevara Y. M., Bower R. G., Schaye J., Furlong M., Frenk C. S., Booth C. M., Crain R., Dalla Vecchia C., Schaller M., Theuns T., 2013, *ArXiv* 1312.0598
- Sawala T., Frenk C. S., Crain R. A., Jenkins A., Schaye J., Theuns T., Zavala J., 2013, *MNRAS*, 431, 1366
- Sawala T., Frenk C. S., Fattahi A., Navarro J. F., Bower R. G., Crain R. A., Dalla Vecchia C., Furlong M., Jenkins A., McCarthy I. G., Qu Y., Schaller M., Schaye J., Theuns T., 2014, *ArXiv e-prints*
- Sawala T., Guo Q., Scannapieco C., Jenkins A., White S., 2011, *MNRAS*, 413, 659
- Schaye J., 2004, *ApJ*, 609, 667
- Schaye J., Dalla Vecchia C., 2008, *MNRAS*, 383, 1210
- Schaye J., Theuns T., Rauch M., Efstathiou G., Sargent W. L. W., 2000, *MNRAS*, 318, 817
- Shen S., Madau P., Conroy C., Governato F., Mayer L., 2013, *ArXiv e-prints*
- Somerville R. S., 2002, *ApJ*, 572, L23
- Springel V., 2005, *MNRAS*, 364, 1105
- Springel V., Di Matteo T., Hernquist L., 2005, *MNRAS*, 361, 776
- Springel V., White S. D. M., Tormen G., Kauffmann G., 2001, *MNRAS*, 328, 726
- Teyssier M., Johnston K. V., Kuhlen M., 2012, *MNRAS*, 426, 1808
- Theuns T., Schaye J., Zaroubi S., Kim T.-S., Tzanavaris P., Carswell B., 2002, *ApJ*, 567, L103
- Wiersma R. P. C., Schaye J., Smith B. D., 2009, *MNRAS*, 393, 99
- Wiersma R. P. C., Schaye J., Theuns T., Dalla Vecchia C., Tornatore L., 2009, *MNRAS*, 399, 574